Editors' Suggestion

Transition from Static to Dynamic Friction in an Array of Frictional Disks

Harish Charan,[1] Joyjit Chattoraj,[2] Massimo Pica Ciamarra,[2] and Itamar Procaccia[1]
[1]Department of Chemical Physics, Weizmann Institute of Science, Rehovot 76100, Israel
[2]School of Physical and Mathematical Sciences, Nanyang Technological University, Singapore 637371, Singapore

(Received 28 August 2019; published 24 January 2020)

The nature of an instability that controls the transition from static to dynamical friction is studied in the context of an array of frictional disks that are pressed from above on a substrate. In this case the forces are all explicit and Newtonian dynamics can be employed without any phenomenological assumptions. We show that an oscillatory instability that had been discovered recently is responsible for the transition, allowing individual disks to spontaneously reach the Coulomb limit and slide with dynamic friction. The transparency of the model allows a full understanding of the phenomenon, including the speeds of the waves that travel from the trailing to the leading edge and vice versa.

DOI: 10.1103/PhysRevLett.124.030602

Introduction.—The transition from static to dynamical friction is an old problem that intrigued the ancient Greeks [1]. Explicitly, Themistius stated in 350 A.D. that "it is easier to further the motion of a moving body than to move a body at rest." The phenomenon is central to many different fields of physics and material science including tribology, performance of microelectromechanical systems, mechanics of fracture, and earthquakes. Despite the considerable amount of work in the modern era starting with Leonardo, Amonton, and Coulomb [2], and culminating with enlightening experiments and simulations in recent years [3–9], the actual instability mechanism that results in this transition is still debated [8,10]. The aim of this Letter is to offer a very simple model for which the prevailing instability mechanism can be understood in full detail. This is done with the conviction that simple models that can be fully understood play an important role in statistical and nonlinear physics where they can often shed light on complex phenomena that may exhibit universal characteristics. Examples are the Ising model for magnetic phase transitions [11] or one-dimensional maps for the onset of chaos [12]. We thus do not attempt to model a specific physical realization, but consider a model that displays the desired transition whose triggering instability and its consequences are manifest and fully understood.

The model is shown in Fig. 1. It consists of N two-dimensional disks of radius R, with their initial center of mass positioned at $x_i = (2i-1)R$, $y_i = R$, $i = 1, \ldots, N$, aligned over an infinite substrate at $y = 0$. Each disk is pressed with an identical force F_y normal to the substrate, providing a very simple model of asperities contacts in more realistic systems. Note that the substrate is totally flat, in contrast to many attempts to explain the desired transition with periodic substrate; see, for example, Ref. [13]. The boundary conditions are periodic such that the disk $i = N$ is in contact with the disk $i = 1$. The forces and torques are annulled by force minimization protocol (see Supplemental Material [14]) to reach mechanical equilibrium. After attaining equilibrium we increase quasistatically a force F_x which is applied at the center of mass of the disk $i = 1$. At some critical value of F_x (see below for details) the system becomes unstable with respect to an oscillatory instability [15,16]. This instability can trigger a transition from static to dynamical friction, which is the subject of this Letter. The instability will be shown to result from the fully Newtonian dynamics of the model, employing standard forces as discussed next, requiring no phenomenological input beyond the definition of the forces. The transition can be seen in a movie provided in the Supplemental Material [14].

Forces.—The interaction forces between the disks and between the disks and the substrate are standard [17]. The normal force is determined by the overlap $\delta_{ij} \equiv 2R - r_{ij}$ between the disks and the compression $\delta_{iw} \equiv R - y_i$ between the disk and the substrate wall, $\boldsymbol{r}_{ij} \equiv \boldsymbol{r}_i - \boldsymbol{r}_j$. We choose a Hertzian force between the disks,

$$\boldsymbol{F}_{ij}^{(n)} = k_n \delta_{ij}^{3/2} \hat{r}_{ij}, \qquad \hat{r}_{ij} \equiv \boldsymbol{r}_{ij}/r_{ij}, \tag{1}$$

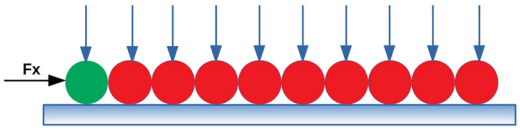

FIG. 1. The model consists of N identical disks (here and in the simulations below, $N = 10$) which interact via Hertz and Mindlin forces between themselves and the substrate below. A constant force F_y is applied to press them against the substrate, and an external force F_x is applied to the first disk, increasing it quasistatically until a pair of complex eigenvalues gets born, signaling an oscillatory instability. From that point on, the Newtonian dynamics takes the system from static to dynamical friction.

and similarly for the normal force between a disk and the substrate. Note that this force is a model force, and although its use is time honored, it should be considered as an effective force since we do not specify the precise deformation of the contact area between the disks and between the disks and the substrate. The tangential force is a function of the tangential displacement $\boldsymbol{t}_{ij}$ between the disks and $\boldsymbol{t}_{iw}$ between the disks and the substrate. Upon first contact between the disks and the substrate, $t_{ij} = t_{iw} = 0$. Providing every particle with the angular coordinate $\boldsymbol{\theta}_i$, the change in tangential displacement is given by

$$d\boldsymbol{t}_{ij} = d\boldsymbol{r}_{ij} - (d\boldsymbol{r}_{ij} \cdot \boldsymbol{r}_{ij})\hat{r}_{ij} + \hat{r}_{ij} \times (Rd\boldsymbol{\theta}_i + Rd\boldsymbol{\theta}_j),$$
$$d\boldsymbol{t}_{iw} = (dx_i + Rd\theta_i)\hat{x}, \tag{2}$$

where $\hat{x}$ is the unit vector parallel to the substrate. For the tangential force we choose the Mindlin model [18], which between the disks reads

$$\boldsymbol{F}_{ij}^{(t)} = -k_t \delta_{ij}^{1/2} t_{ij} \hat{t}_{ij}, \tag{3}$$

with a similar definition for the tangential force between the disk and the substrate. The tangential forces satisfy the Coulomb condition,

$$\boldsymbol{F}_{ij}^{(t)} \leq \mu \boldsymbol{F}_{ij}^{(n)}, \tag{4}$$

where $\mu = 10$ is the friction coefficient. For technical purpose we smooth out the Coulomb law such that the tangential force will have smooth derivatives; we choose

$$\boldsymbol{F}_{ij}^{(t)} = -k_t \delta_{ij}^{1/2} \left[1 + \frac{t_{ij}}{t_{ij}^*} - \left(\frac{t_{ij}}{t_{ij}^*}\right)^2\right] t_{ij} \hat{t}_{ij}, \qquad t_{ij}^* \equiv \mu \frac{k_n}{k_t} \delta_{ij}. \tag{5}$$

Now the derivative of the force with respect to t_{ij} vanishes smoothly at $t_{ij} = t_{ij}^*$ and Eq. (4) is fulfilled.

Dynamics and transition.—The dynamics is Newtonian; we denote the set of coordinates $\boldsymbol{q}_i = \{\boldsymbol{r}_i, \boldsymbol{\theta}_i\}$ as

$$m \frac{d^2 \boldsymbol{r}_i}{dt^2} = \boldsymbol{F}_i(\boldsymbol{q}_{i-1}, \boldsymbol{q}_i, \boldsymbol{q}_{i+1}), \qquad q_{N+1} = q_1, \tag{6}$$

$$I \frac{d^2 \boldsymbol{\theta}_i}{dt^2} = \boldsymbol{T}_i(\boldsymbol{q}_{i-1}, \boldsymbol{q}_i, \boldsymbol{q}_{i+1}), \tag{7}$$

where m and I are the mass and moment of inertia of the ith disk, $\boldsymbol{F}_i$ is the total force on disk i, and $\boldsymbol{T}_i$ is the torque on that disk. Below, time is measured in units of $\sqrt{m2Rk_n}$ and length in units of $2R$. Although the simulations were performed for a wide range of parameters, we present results for $k_n = 2000$, $k_t = 2k_n/7$, $F_y = 0.1$. The conditions for mechanical equilibrium are $\boldsymbol{F}_i = \boldsymbol{T}_i = 0$, and the stability of an equilibrium state is determined by the Jacobian matrix

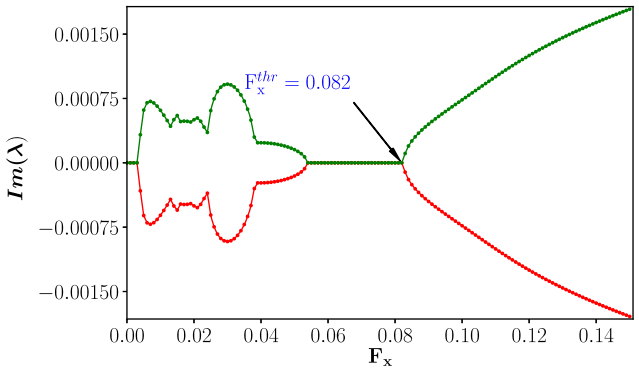

FIG. 2. Two examples of a bifurcation of a pair of imaginary parts of eigenvalues upon increasing the external force F_x. A pair of real eigenvalues coalesces when the pair of imaginary eigenvalues bifurcates. The first bifurcation results in an oscillatory instability, but the force F_x is not sufficient to trigger a transition to dynamical friction. The second does.

$$J_{ij}^{\alpha\beta} \equiv -\frac{\partial \tilde{F}_i^\alpha}{\partial q_j^\beta}, \qquad \tilde{\boldsymbol{F}}_i \equiv \sum_j \tilde{\boldsymbol{F}}_{ij}, \tag{8}$$

where $\boldsymbol{q}_j$ stands for either a spatial position or a tangential coordinate and $\tilde{\boldsymbol{F}}_i$ stands for either a force or a torque. The explicit calculation of the Jacobian matrix for the present model is presented in the Supplemental Material [14]. For our purpose here it is enough to note that the Jacobian matrix is real but not symmetric, and therefore it can have pairs of complex eigenvalues which necessarily lead to an oscillatory instability [15,16]. Even if initially all the eigenvalues are real and the system is stable, by increasing the external force F_x we always reach a threshold value of this force where a pair of complex eigenvalues is born. Details of this protocol and code [19] are in the Supplemental Material [14]. We should add that changing the material parameters like the force constants or the friction coefficient changes the value of F_x where instability sets in but does not change the nature of the results presented below.

Instability and dynamics.—The birth of the instability is demonstrated in Fig 2. Note that this figure exhibits two events of birth of a complex conjugate pair of eigenvalues. The first complex pair dies out with increasing F_x without triggering a transition to dynamical friction. The difference in dynamical response is presented in Fig. 3, which shows the mean-square displacement $M(t) = (1/10)\sum_{i=1}^{10} |\boldsymbol{r}_i(t) - \boldsymbol{r}_i(0)|^2$. The protocol resulting in these dynamics is spelled out in detail in the Supplemental Material [14]. For the two external forces $F_x = 0.03$ and 0.04, the oscillatory instability exists, but the mean-square displacement becomes stationary at a minute fraction of the disk radius (about 10^{-5}), indicating static friction with charging of t_{iw} but without transition to dynamical friction. For $F_x = 0.062$, all the eigenvalues of $\boldsymbol{J}$ are real, there is no instability, and $M(t)$ never increases. For $F_x = 0.083$, the system is in the second regime of

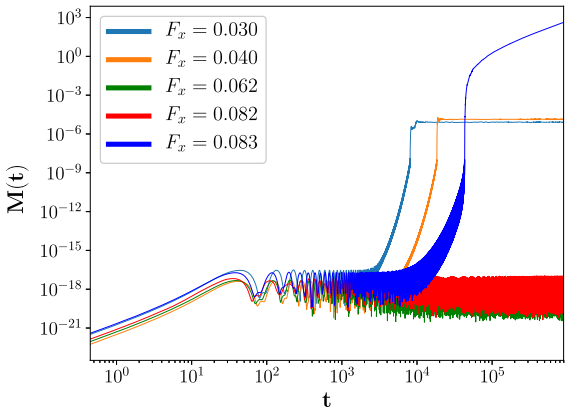

FIG. 3. Dynamical response of $M(t)$ at various values of F_x. The two lowest values are within the range of existence of an oscillatory instability (see Fig. 2), but F_x is not large enough to trigger a transition to dynamical friction. For $F_x = 0.062$, the system is stable and $M(t)$ remains minute. The largest value of $F_x = 0.083$ is after the birth of the new pair of complex eigenvalues, and now the oscillatory instability triggers the transition to dynamical scaling.

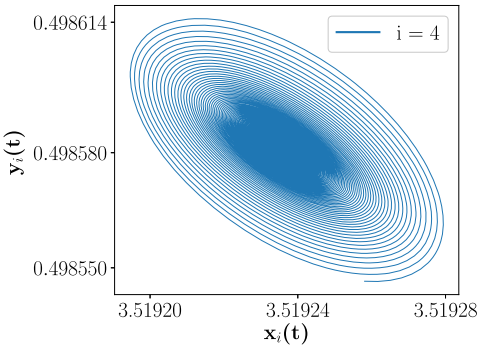

FIG. 4. The actual trajectory in the x-y plane (for $t \approx 17500$) that is induced by the instability. Here we show the fourth grain ($i = 4$), but this is representative for all grains.

oscillatory instability, which is now developing strongly, bringing $M(t)$ to about $10^{-2}R$, where for the first time the Coulomb law is breached at the contact with the substrate, and subsequently $M(t)$ increases linearly in time with a fixed average velocity.

The mechanism of the transition is understood by watching the typical trajectories of the centers of mass of the disks following the instability. An example pertaining to the fourth disk is shown in Fig. 4, and is representative for all the other disks. A spiral of growing amplitude in the x-y plane leads in time to an increase in y_i to the point that breaching the Coulomb law at the contact with the substrate becomes inevitable. In consequence, the tangential forces at contact fail to oppose the external force F_x and a transition to dissipative dynamical friction can take place. The breaching of the Coulomb law is however not simultaneous. The actual onset of dynamic friction is in close accord with experimental and simulational reports [3,5,8]. The first disk reaches the Coulomb limit at some time τ_1, and consequently a forward wave of such events runs through the system, with the second, third, fourth, etc. disk reaching the Coulomb limit at times τ_i with $\tau_{i+1} > \tau_i > \tau_1$ and i being the index of the disk. While each realization is somewhat stochastic, averaging over 25 realizations as shown in Fig. 5 indicates that

$$V_1(F_x)(\tau_i - \tau_1) \approx x_i, \tag{9}$$

with a wave speed $V_1(F_x)$ depending on the external force F_x. In Fig. 5, upper panel, τ denotes the time that a disk breaches the Coulomb law for the first time and $x(\tau)$ is the position of the disk when this takes place. For $F_x = 0.083$, 0.087, 0.090, the corresponding velocity of this front is 0.0014 ± 0.00013, 0.0022 ± 0.00015, and $0.0028 \pm 8 \times 10^{-5}$. These velocities are explained below.

The actual sliding begins at the leading (last) disk, with a backward wave of sliding traveling from the last to first disk. This is also in accord with experimental and simulational

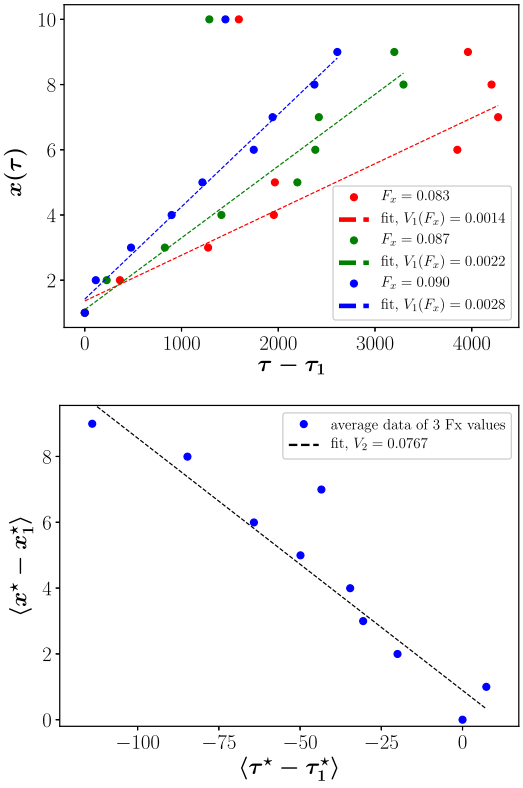

FIG. 5. Upper panel: The wave of breaching of the Coulomb law, starting with the first disk and ending with the last. Every realization is noisy, but averaging on 25 realizations yields this plot which supports a wave velocity $V_1(F_x)$ that depends on the external force F_x. Lower panel: The wave of actual sliding, starting with the last disk and ending with the first. This backward running wave has a velocity V_2 that does not depend on the external force F_x.

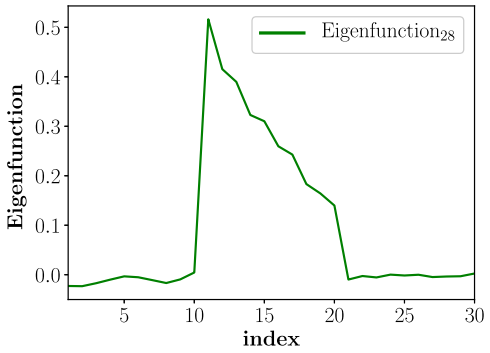

FIG. 6. Projection of the shear-wave eigenfunction of the Jacobian matrix on the degrees of freedom q_ℓ, x modes for $\ell = 1$–10, y modes for $\ell = 11$–20, and angular modes for $\ell = 21$–30. This mode is predominantly a y shear wave that is responsible for initiating the sliding motion. The wavelength of this up-down shear wave is approximately 2.

observations [5,8]. The speed of the backward wave is independent of F_x, indicating that it is an inherent elastic wave, as is explained below. It is also in agreement with observations that the speed V_2 of the backward wave of sliding is much faster than V_1 [3]. In the lower panel of Fig. 5 the times τ^* are measured backwards from the first sliding of the last disk, and x^* is the position where the sliding occurs. Since the velocity of the backward wave is independent of F_x, the lower panel of Fig. 5 is obtained by averaging the data from simulations at the same three values of F_x as the ones shown in the upper panel.

Theory.—To understand the wave speeds, we discuss first the backward wave of detachment which is dominated by an elastic transverse wave of up-down motion in the y direction. Examining the 30 eigenfunctions of the Jacobian matrix $\boldsymbol{J}$, one identifies only one which consists of a pure y transverse wave; see Fig. 6. This eigenfunction has no projection on either longitudinal or angular degrees of freedom. It has an eigenfrequency $\omega \approx 0.235$ and a wavelength of approximately 2. Thus the associated k vector is $k \approx 2\pi/2 \approx \pi$, determining a velocity $V_2 \approx 0.235/\pi \approx 0.075$ in excellent agreement with the measured value of the backward velocity.

The forward wave of Coulomb breaching is not related to the internal elastic waves in the system. Rather, it is related to the imaginary part of the pair of complex eigenvalues, which governs the exponential growth rate of the spiral trajectories and therefore the push by the ith disk on the $(i+1)$th disk, resulting in breaching the Coulomb threshold. Indeed, while the backward wave speed is basically independent of F_x, the forward wave speed must be a function of F_x since the imaginary part of the eigenvalues grows with increasing F_x. For the three values of F_x shown in the upper panel of Fig. 5, the imaginary part of the associated eigenvalue is 0.00024,0.00077, and 0.001, respectively. Using the values of the velocities measured for the three different values of F_x, we compute the ratios

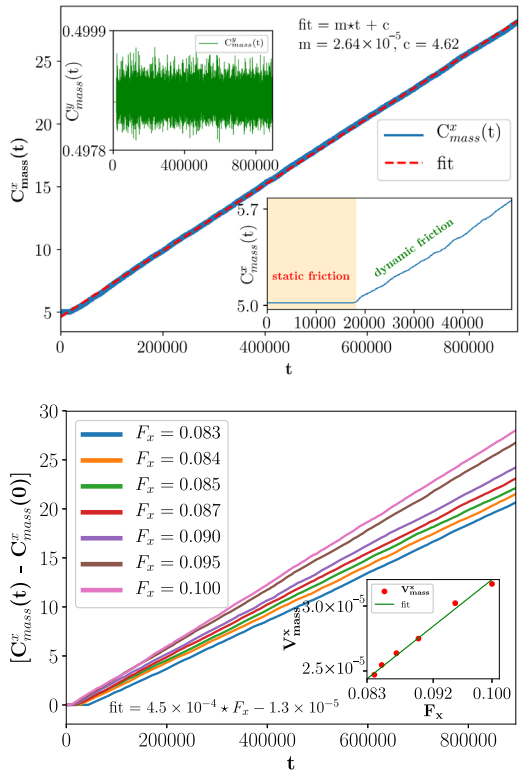

FIG. 7. The transition from static to dynamical friction as measured by the dynamics of the center of mass. Upper panel: The motion of the x component of the center of mass for $F_x = 0.087$. The upper inset shows the y component of the center of mass that oscillates without growth. The lower inset shows the transition itself from static to dynamics. Lower panel: The dynamics of the x component of the center of mass for different values of F_x. The inset shows how the velocity of the center of mass depends on F_x.

of these velocities to the growth rates to find an approximate constant value 4.3 ± 1.5.

The transition as seen from the dynamics of the center of mass of the whole system is shown in the upper panel of Fig. 7. Here the x and y components of the center of mass are defined as $C^x_{\rm mass} \equiv (1/N)\sum_i^N x_i$ and equivalently for y. In the upper inset we show $C^y_{\rm mass}$, which is oscillating without growth. The main figure displays $C^x_{\rm mass}$ as a function of time. The lower inset shows the transition itself, which on the scale shown appears like a simple first order transition from static to dynamics with a fixed velocity $V^x_{\rm mass}$, hiding all the microscopic richness discussed above. In the lower panel we display the dependence of the constant velocity in the dynamic friction regime on the external force F_x. The inset indicates a liner relation between the two, with the best fit reading

$$V^x_{\rm mass} \approx -1.3 \times 10^{-5} + 4.5 \times 10^{-4} F_x. \qquad (10)$$

Summary.—The rich physics associated with the transition from static to dynamical friction is demonstrated

using a very simple model of N disks on a flat substrate, interacting via the often used Hertz and Mindlin forces. By increasing the external force F_x, Newtonian dynamics without further phenomenological assumptions result in an oscillatory instability that ends up with the observed transition. In agreement with much more complicated experimental and simulational examples, the transition is associated with forward and backward running waves of events that accompany the transition. An advantage of the simple model is that the instability, its development, and the wave speeds observed can all be understood in full detail. It should be of utmost interest to examine the mechanism described here also in experimental contexts, since we expect the instability to exist equally well in two- and in three-dimensional contexts [20].

This work has been supported by the ISF-Singapore program and by the U.S.-Israel BSF. We thank Eran Bouchbinder and Yuri Lubomirsky for useful discussions on wave propagations. J. C. and M. P. C. were supported by the Singapore Ministry of Education through the Academic Research Fund (Tier 2) MOE2017-T2-1-066 (S) and the National Suprecomputing Center Singapore (NSCC) for computational resources.

[1] S. Sambursky, *The Physical World of Late Antiquity* (Princeton University Press, Princeton, NJ, 2014), pp. 65–66.
[2] E. Popova and V. L. Popov, Friction and wear in machinery **3**, 183 (2015).
[3] S. M. Rubinstein, G. Cohen, and J. Fineberg, Nature (London) **430**, 1005 (2004).
[4] O. M. Braun, I. Barel, and M. Urbakh, Phys. Rev. Lett. **103**, 194301 (2009).
[5] O. Ben-David, G. Cohen, and J. Fineberg, Science **330**, 211 (2010).
[6] R. Sahli, G. Pallares, C. Ducottet, I. E. Ben Ali, S. Al Akhrass, M. Guibert, and J. Scheibert, Proc. Natl. Acad. Sci. U.S.A. **115**, 471 (2018).
[7] A. Vanossi, N. Manini, M. Urbakh, S. Zapperi, and E. Tosatti, Rev. Mod. Phys. **85**, 529 (2013).
[8] Y. Bar-Sinai, R. Spatschek, E. A. Brener, and E. Bouchbinder, Phys. Rev. E **88**, 060403(R) (2013).
[9] S. Bonfanti, A. Taloni, C. Negri, A. L. Sellerio, N. Manini, and S. Zapperi, J. Phys. Chem. Lett. **8**, 5438 (2017).
[10] J. Trømborg, J. Scheibert, D. S. Amundsen, K. Thøgersen, and A. Malthe-Sørenssen, Phys. Rev. Lett. **107**, 074301 (2011).
[11] H. E. Stanley, *Phase Transitions and Critical Phenomena* (Clarendon Press, Oxford, 1971).
[12] M. J. Feigenbaum, J. Stat. Phys. **19**, 25 (1978).
[13] Y. Braiman, F. Family, and H. G. E. Hentschel, Phys. Rev. E **53**, R3005 (1996).
[14] See Supplemental Material at http://link.aps.org/supplemental/10.1103/PhysRevLett.124.030602 for analytical calculation of the force and torque derivatives and for the computational protocol.
[15] J. Chattoraj, O. Gendelman, M. Pica Ciamarra, and I. Procaccia, Phys. Rev. Lett. **123**, 098003 (2019).
[16] J. Chattoraj, O. Gendelman, M. P. Ciamarra, and I. Procaccia, Phys. Rev. E **100**, 042901 (2019).
[17] P. A. Cundall and O. D. L. Strack, Gotechnique **29**, 47 (1979).
[18] R. Mindlin, Trans. ASME **16**, 259 (1949).
[19] S. Plimpton, J. Comput. Phys. **117**, 1 (1995).
[20] S. Bonfanti, J. Chattoraj, R. Guerra, I. Procaccia, and S. Zapperi, arXiv:1909.05070.